Citrus Black Spot Detection using Hyperspectral Imaging[†]

Dae G. Kim[1], Thomas F. Burks[1]*, Mark A. Ritenour[2], and Jianwei Qin[3]

[1]University of Florida, Ag & Bio Eng., 1740 Rogers Hall, Museum Road, Gainesville, FL 32611

[2]University of Florida, IRREC, 2199 S. Rock Road, Ft. Pierce, FL 34945

[3]U.S. Department of Agriculture, 10300 Baltimore Avenue, Beltsville, MD 20705

Additional index words. spectral information divergence, spectral angle mapper, machine vision, classification algorithms

The viability of the Florida fresh citrus industry is threatened by yet another citrus disease called citrus black spot (CBS), which has arrived as the industry battles two other recently introduced and devastating diseases (citrus canker and Huanglongbing). CBS symptoms make the fruit unacceptable for some important fresh fruit export markets such as the European Union. Therefore, it is imperative to identify fruits that are infected with CBS prior to distribution. This paper describes the development of a hyperspectral imaging approach for identifying fruits infected with CBS. Hyperspectral images were taken of healthy fruit and those with CBS symptoms or other potentially confounding peel conditions such as greasy spot, wind scar, or melanose. Spectral Angle Mapper (SAM) and Spectral Information Divergence (SID) hyperspectral analysis approaches were used to classify fruit samples into two classes: CBS or non-CBS. Results showed that CBS classification accuracy using the SAM approach was 97.90%, and SID classification accuracy was 97.14%. The combination of the hyperspectral images and the two classification approaches (SID and SAM) have proven to be effective in recognizing CBS in the presence of other potentially confounding fruit peel conditions.

In recent years citrus black spot (CBS) has become another exotic disease threatening fresh Florida citrus growers and shippers similar to citrus canker and Huanglongbing. Once citrus trees are infected with CBS, their fruit yield and visual quality are greatly reduced and fruits with CBS symptoms are not acceptable in some important fresh fruit export markets, such as those of the European Union (Chung et al., 2009). Therefore, it is important to control this disease in the field to preserve profitable production and to detect and eliminate infected fruit at the packinghouse to maintain marketability.

CBS symptoms can be quite variable and are identified by cosmetic lesions on the fruit peel (Dewdney, 2010). CBS hard spot lesions, the most common symptom type, begin as small orange or red spots with black margins that enlarge and become necrotic. Other symptoms of CBS on citrus fruit peel include virulent spot, cracked spot, and false melanose (Dewdney et al., 2011). Detecting fruits infected with CBS can also help in controlling the spread of this disease to areas that are currently free of CBS. The design and implementation of technologies that can efficiently detect CBS disease will greatly aid in the control effort.

The identification of various crops and plant using machine vision and image processing techniques has been studied by numerous researchers. Jimenez et al. (2000) surveyed several computer vision approaches for locating fruit in trees for robotic harvesting. Regunathan and Lee (2005) identified fruit count and size using machine vision and an ultrasonic sensor. Burks et al. (2000) developed a method for classifying weed species using color texture features and discriminant analysis. Tang et al. (1999) developed a texture-based weed classification method using Gabor wavelets and neural networks for real-time selective herbicide application. Pydipati et al. (2006) identified citrus disease

using the co-occurrence matrix method, (CCM) texture feature method, and a discriminant analysis. Du et al. (2006) described five different texture feature methods, including the common first-order gray-level statistics (FGLS), run length matrix (RLM), gray-level co-occurrence matrix (GLCM), fractal dimension (FD), and wavelet transform (WT) based methods.

In recent years, optical techniques have been used widely in the food processing and inspection application. In particular, hyperspectral imaging technologies have had growing interest for use in quality and safety inspection of food and agricultural products (Sun, 2010). Previous research has demonstrated hyperspectral imaging technologies and applications for agricultural products. Jiang et al. (2007) used hyperspectral fluorescence imaging to analyze the differences between walnut shells and meat. A hyperspectral fluorescence imaging system scanned samples at 79 different wavelengths ranging from 425 nm to 775 nm with 4.5-nm increments, later data redundancy was reduced through principal component analysis (PCA). Zhang et al. (2005) suggested a novel classification approach for distinguishing healthy and fungal infected wheat kernels during storage. The research showed the potential use of NIR hyperspectral imaging in grain quality assessment. The research used NIR hyperspectral imaging and support vector machine (SVM) for identifying the fungi that caused the infection. Kim et al. (2001) researched a method for using hyperspectral data to identify wavebands to be used in multispectral detection systems, and evaluated spatial and spectral responses of hyperspectral reflectance images of fecal-contaminated apples. Lee et al. (2005) used the hyperspectral imaging technique to detect defects on apple peel after harvest using a wavelength selection method.

In hyperspectral image classification approaches, a spectral angle mapper (SAM) and spectral information divergence (SID) classification that measures the spectral similarity between two spectra has been applied to various agricultural products and systems. Park et al. (2007) used SAM algorithms to detect fecal

and ingesta contaminants on the surface of poultry carcasses. Qin et al. (2009) introduced the detection of citrus canker using SID classification methods. Yang et al. (2006) used the SAM method on airborne hyperspectral imagery for mapping yield variability.

This paper reports on work to develop a hyperspectral-based machine vision system for detecting and distinguishing fruit CBS symptoms from other common citrus peel conditions. This approach could be used in an off-line fruit blemish detection system, or could be used as the basis for the development of a real-time multi-spectral detection system. The overall objective of this research was to develop and compare the performance of two hyperspectral classification methods, spectral angle mapper (SAM) and spectral information divergence (SID), for detection of CBS using a hyperspectral imaging system.

Methodology

Fruit sample collection

'Valencia' oranges were hand-picked from citrus groves near Immokalee in southwestern Florida in Apr. 2010. The fruit samples included marketable fruit and those with symptoms of CBS, greasy spot, melanose, and wind scar. Representative images for each peel condition are shown in Figure 1. All fruit samples were washed with a mild soap to remove surface dirt before imaging.

To maximize the number of hyperspectral images collected from the limited number of CBS samples, three faces of each fruit (with 120° rotation intervals) were collected as shown in Figure 2. Table 1 illustrates the sample distribution for this study, with 135 CBS and 390 non-CBS for a total of 525 samples.

Hyperspectral image acquisition

A hyperspectral line-scan imaging system, as shown in Figure 3, was used for acquiring hyperspectral images of the fruit samples. This system was based on design recommendations by Kim et al. (2001). The imaging system consisted of an electron-multiplying charge-coupled-device (EMCCD) camera (Luca, Andor Technology Inc., South Windsor, CT) with imaging spectrograph (ImSpector V10E, Spectral Imaging Ltd., Oulu, Finland) and a C-mount lens (Rainbow CCTV S6X11, International Space Optics, S.A., Irvine, CA), a pair of halogen line lamps (21 V, 150 W) powered with a DC voltage regulated power supply (Dolan-Jenner Industries, Inc., Lawrence, MA). This equipment was placed inside a dark box to eliminate undesirable external light. The reflectance light source consists of two 21-V, 150-W halogen lamps powered with a DC voltage regulated power supply (TechniQuip, Danville, CA). The light was transmitted through optical fiber bundles toward line light distributors. Two line lights are arranged to illuminate the Image Field Of View (IFOV).

Fig. 1. Representative images for each peel condition.

Fig. 2. Three faces of each fruit with 120° interval.

Table 1. The number of citrus black spot (CBS) and other conditions.

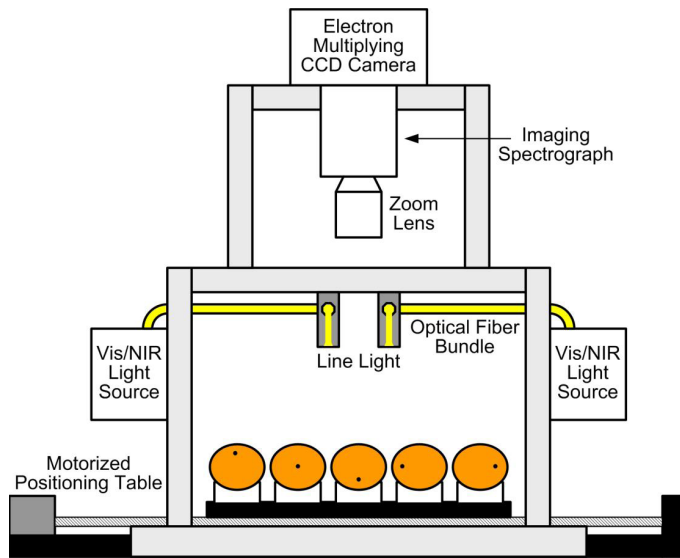| Class	Symptoms	No.	Total
CBS disease	Black spot	135	135
No CBS disease	Greasy spot	90	390
	Market	90	
	Melanose	105	
	Wind scar	105	

Fig. 3. Hyperspectral line-scan imaging system.

The EMCCD has 1004 × 1002 pixels and a double-stage Peltier device to cool to –80 °C. An imaging spectrograph is based on prism-grating- prism principle. It has a slit 2.8 nm long and 30 μm wide. Through the slit, light from the scanned line is dispersed by a prism-grating prism device and projected onto the pixels of EMCCD detector. A two-dimensional image is generated with the spatial dimension along the horizontal axis and the spectral dimension along the vertical axis of the EMCCD. A programmable, motorized positioning table (BiSlide-MN10, Velmex Inc., Bloomfield, NY) moves citrus samples (five for each run) transversely through the line of the IFOV. For five fruit samples 1740 line scans were performed, and 400 pixels covering the scene of the fruit at each scan were saved, generating a 3-D hyperspectral image cube with the spatial dimension of 1740 × 400 for each band.

The hyperspectral imaging software to transfer data and parameterization was developed using the Andor Software Development Kit (SDK, Luca, Andor Technology Inc.) for the hyperspectral line scan imaging system. An Hg-Ne spectral calibration lamp (Oriel Instruments, Stratford, CT) was used to investigate spectral calibration of the system. Because of low light output in the visible region less than 450 nm, and low quantum efficiency of the EMCCD in the NIR region beyond 930 nm, the wavelength range between 451.67 nm and 927.71 nm was used (totaling 92 bands with a spectral resolution of 5.2 nm).

Image processing

FLAT-FIELD CORRECTED IMAGES. Flat-field corrections were performed on the hyperspectral images to obtain the relative reflectance prior to image analysis and image processing for classification. Equation 1 was used for the flat-field correction to obtain the relative reflectance R for the 92 spectral bands. Flat-field correction technique can reduce uneven illumination and distortion.

$$R(w) = \frac{R_{sample}(w) - R_{dark}(w)}{R_{White}(w) - R_{dark}(w)} \times r$$

where R(w) is the relative reflectance, $R_{sample}(w)$ is the original sample image data range of 0–16383 (14-bit EMCCD), $R_{white}(w)$ is the reference image acquired from the white Spectralon calibration panel, $R_{dark}(w)$ is the dark current image obtained with a cap covering the camera lens, w is the wavelength, and r is the reflectance factor of the calibration panel. The actual reflectance factor for the Spectralon panel is about 99% in the wavelength range measured by the hyperspectral imaging system, however a reflectance factor of 100% was used in this study for simplicity. The relative reflectance R(w), which has a value between 0 and 1, was then scaled to a range of 0 to 10,000 to increase the dynamic range of the adjusted reflectance.

To reduce image noise and processing time, the fruit peel area was separated from the background by creating a fruit parameter mask. The mask was created, by manual inspection, using a threshold value determined from the hyperspectral image which gave the largest contrast between the fruit and background. After masking the background, the image spatial resolution was reduced by half by resampling which yielded equivalent spatial resolution in the horizontal and vertical dimensions. These image processing steps served several important purposes: 1) it reduces the computational burden of extraneous features outside region of interest, 2) it tends to improve the performance of classification algorithms, and 3) it reduces memory and storage demands. The resulting pre-processed images then became the test samples to be used in classification studies to validate the performance of SID and SAM algorithms for identifying CBS conditions on fruit.

Hyperspectral image analysis and classification

The spectral angle mapper (SAM) and spectral information divergence (SID) algorithms are two important supervised classification methods used in analyzing the spectral characteristics of agricultural products. They are described in the following section.

A. SPECTRAL ANGLE MAPPER. Figure 4 illustrates that the main concept of SAM is to calculate the angle between endmember spectra and target spectra as vectors in a space with dimensionality equal to the number of bands (Yang et al., 2006). The formula of spectral angle (θ) is calculated as:

$$\theta = cos^{-1}\left(\frac{\sum_{\lambda=1}^{M} \rho_\lambda \rho'_\lambda}{L_\rho L_{\rho'}}\right)$$

where M is the number of spectral bands, ρ_λ is the reflectance of endmember spectrum, ρ'_λ is the reflectance of a target spectrum,
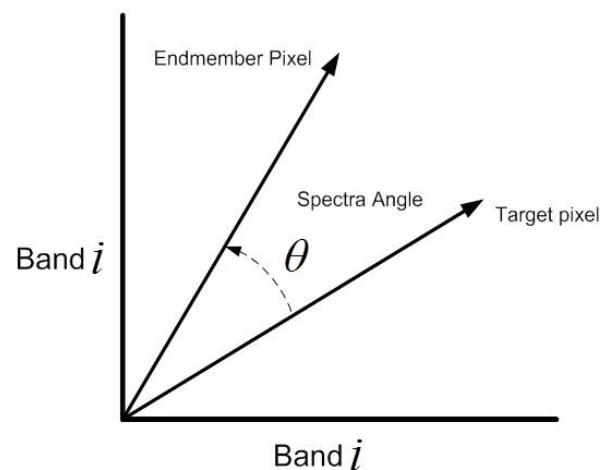

Fig. 4. The angle between endmember spectra and target spectra as vectors in a space.

L_ρ is the length of the endmember vector, and $L_{\rho'}$ is the length of the target spectrum vector.

The length of the endmember vector and the target spectrum vector are calculated as:

$$L_\rho = \sqrt{\sum_{\lambda=1}^{M} \rho_\lambda^2}, \quad L_{\rho'} = \sqrt{\sum_{\lambda=1}^{M} {\rho'_\lambda}^2}$$

After finding the spectral angle (θ), the spectral angle is compared with a threshold value. If the threshold is below the angle, the target spectrum is determined as classifying to the end member class (Shippert, 2003).

B. Spectral Information Divergence. While SAM is a deterministic method, SID is a probabilistic method that allows for variations in pixel measurements, where probability is measured from zero to a user-defined threshold (Du et al., 2004). Chang (1999) described the derivation of spectral information divergence (SID).

The hyperspectral pixel vector is given by

$X = (x_1, x_2, x_3, ..., x_n, ..., x_N)^T$

Each component x can be modeled as a random variable by defining an appropriate probability distribution. Due to the nature of reflectance, assume that all component x_i's in X are non-negative. Thus, the probability measure can be defined as:

$$p_j = \frac{x_j}{\sum_{n=1}^{N} x_n}$$

and the desired probability vector is

$$P = \{p_l\}_{l=1}^{L}.$$

For an information theory to capture relationship and correlation between two hyperspectral pixel vectors, another pixel vector

$Y = (y_1, y_2, y_3, ..., y_n, ..., y_N)^T$

with the probability distribution given by

$$Q = \{q_l\}_{l=1}^{L} \text{ and } q_j = y_j / \sum_{n=1}^{N} y_n.$$

Thus, spectral information divergence (SID) can be given by:

$SID(X,Y) = D(X\|Y) + D(Y\|X)$

where $(X\|Y)$, called as the relative entropy of Y with respect to X, is defined by

$$D(X \| Y) = \sum_{l=1}^{L} p_l \, log(\frac{p_l}{q_l}) \text{ and } D(X \| Y) = \sum_{l=1}^{L} q_l \, log(\frac{q_l}{p_l})$$

Therefore, the value of SID shows the use of the relative entropy and the similarity between two spectral pixels.

Black Spot classification. A detailed flowchart illustrating the SAM and SID classification algorithms is shown in Figure 5. After calculating the relative hyperspectral reflectance images for all the wavelengths (483 to 959 nm), the relative reflectance image was scaled to the range of 0 to 10,000. In the next step, the mask template is used to eliminate background noise and reduce image boundary size. Once the image background was masked (background reflectance thresholded to zero), the image spatial
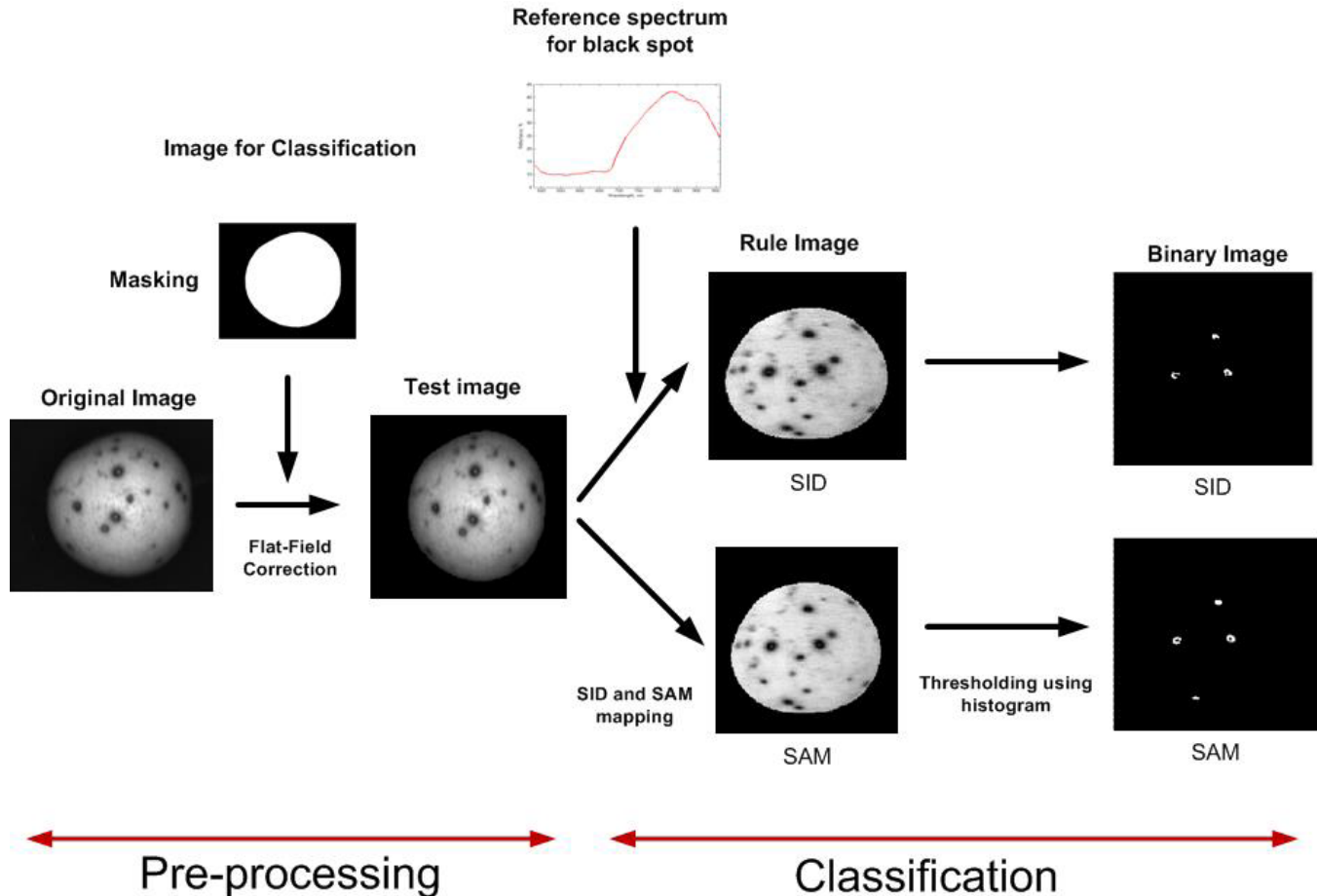

Fig. 5. A detailed illustration of SAM and SID classification algorithms.

resolution was reduced by half by resampling, thus yielding comparable spatial resolutions for vertical and horizontal dimensions. Next, the spectral similarity for SAM and SID based classification algorithms was determined between endmember (CBS) and target (random test fruit sample) spectrum by calculating the SAM angle and SID divergence. In this study, the mean reflectance spectra from 3 × 3 pixel regions of interest (ROIs) from 10 CBS sample regions were used for describing endmember spectra. The ROIs were randomly selected from CBS infected image samples by manually selecting the 3 × 3 window inside the boundary of a CBS lesion. Since the endmember spectra was composed of the mean of the actual 10 CBS samples, it created a unique endmember,

thus allowing the original 10 CBS samples to be returned to the data set and used for testing. The mean and standard deviation from endmember spectra are illustrated in Figure 6. After applying SID and SAM mappings to the hyperspectral image of each test sample, rule images were used to separate CBS lesions from other fruit peel conditions. Representative rule images from SID and SAM mapping for the hyperspectral images are shown in Figure 7.

Results and Discussion

Spectral characteristics of black spot and other conditions

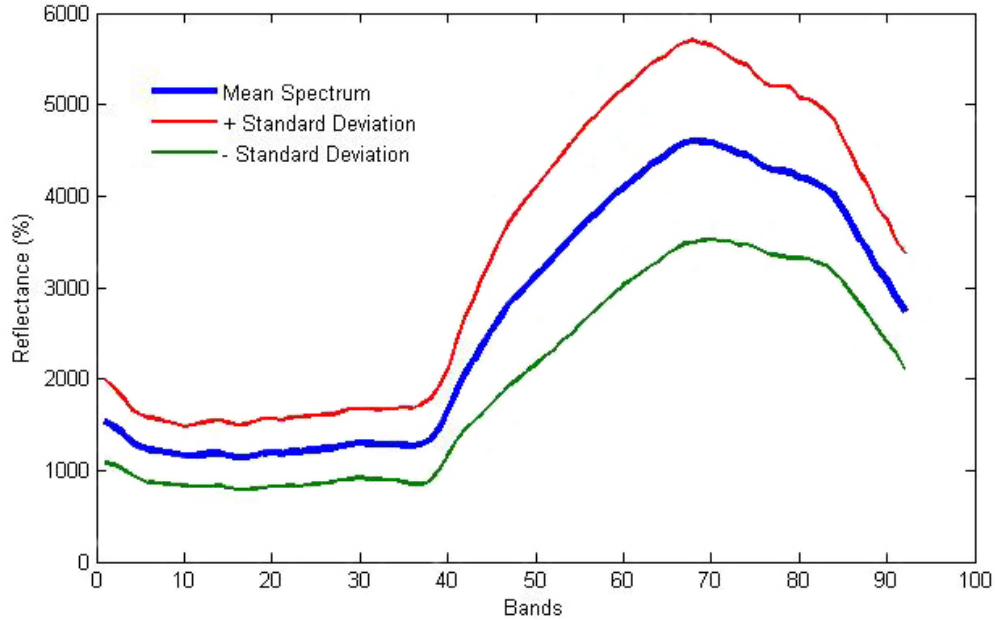The reflectance spectra of the various peel conditions (CBS,

Fig. 6. The variability in endmember spectra as illustrated by mean and standard deviation from black spot endmember spectra.
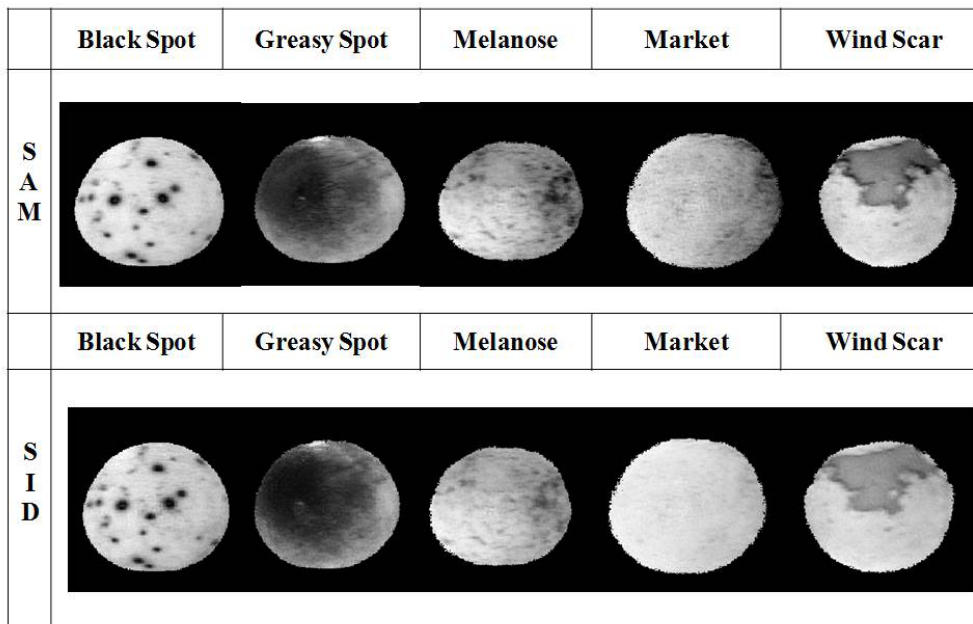

Fig. 7. Representative rule images from SID and SAM mapping for the hyperspectral images.

market quality and other diseases) over the wavelength range from 483 to 959 nm are shown in Figure 8. These plots were developed using the mean of 10 CBS spectra from different hyperspectral image samples. The spectra of each peel condition shows a similar pattern, regardless of the surface conditions, with the difference appearing as shifts either upward or downward depending on the peel conditions reflectance characteristics.

All the spectra plots feature a local minimum around 675 nm, due to difference of light absorption of chlorophyll and carotenoid between CBS and other conditions. As shown in Figure 8, the spectra from market fruit had the highest slope in reflectance vs. wavelengths from 500 nm to 575 nm, while other disorders gradually increased in reflectance in this region. CBS remained fairly flat in this region, having a consistently lower reflectance than the other conditions. The spectra reflectance values of other disorders generally are bounded between the spectra of CBS (lowest) and market (highest) for wavelengths between 550 nm to 650 nm with reflectance ranging between 12% and 50%. In the region from 700 nm to 800 nm, the reflectance ranges between 40% and 70%. Reflectance spectra from hyperspectral images were extracted using ENVI 4.3 (ITT Visual Information Solutions, Boulder, CO).

SID and SAM based classification

SID and SAM mappings were generated using the end spectra of CBS with the resulting rule images showing enhanced CBS regions. The SAM angle and SID divergence values of CBS ranged from 0.01 to about 0.1. Based on these values, a threshold algorithm was used to generate the binary classification image, which separated CBS from other conditions by setting each pixel to either "1" for CBS or "0" for the other classes. Figure 5 shows a sample binary image resulting from the threshold operation where the CBS regions are represented by the white pixels.

SID-based CBS classification results are shown in Table 2 for six different threshold values. Classification trials were conducted by incrementally increasing the SID threshold value from the lowest value of 0.01(see Fig. 8) to the highest value

of 0.06 at a step increment size of 0.01. As indicated in Figure 9(a), the value of 0.04 provided the best overall performance of 97.14%. When the threshold was changed from 0.01 to 0.04, the classification accuracy increased linearly from 74.28% to 97.14%, respectively. However, the overall classification accuracy peaked at threshold value 0.04 and decreased as the threshold value was further increased to 0.05. Based on the results shown in Table 3, the SID classification accuracy for "CBS" class was 98%, while the accuracy for "No CBS" class was 96.92%. Only three CBS samples were misclassified at the threshold value of 0.04, while 12 non CBS class samples were misclassified (eight greasy spot and four wind scar samples). All melanose and market samples were correctly classified at a 0.04 SID threshold. It should be noticed as the threshold value increases to the upper limit, that although overall classification accuracy decreases, the accuracy of CBS detection actually increases. Therefore decisions can be made to optimize for CBS detection, rather than overall classification.

During the SAM classification trials, shown in Table 4, the SAM threshold values were changed from 0.06 to 0.11 by a 0.01 increment. Figure 9(b) shows the effect that changing the threshold had on overall classification accuracy, which increased from 81% (0.06) to 97.9% (0.09) at the peak, and then decreased to about 90%. SAM showed similar classification accuracy characteristics to that of SID , however SAM mapping had a higher overall accuracy in the tested range. As shown in Table 5, for the best classification result, the classification accuracies for 'CBS' class, and 'No CBS' class were 98% and 97.95%, respectively. There were three misclassified samples for 'CBS' class, and eight misclassified samples for 'Non CBS' class which consisted of greasy spot samples alone. The other three non-CBS classes ('Market', 'Wind Scar', and 'Melanose') had perfect classification results (100%). The plot of reflectance spectra in Figure 8 illustrated that greasy spot was very close to those of CBS, which contributed to the misclassification. Imaging parameters that will enhance the difference between the CBS samples and other confounding conditions such as greasy spot will be investigated in future
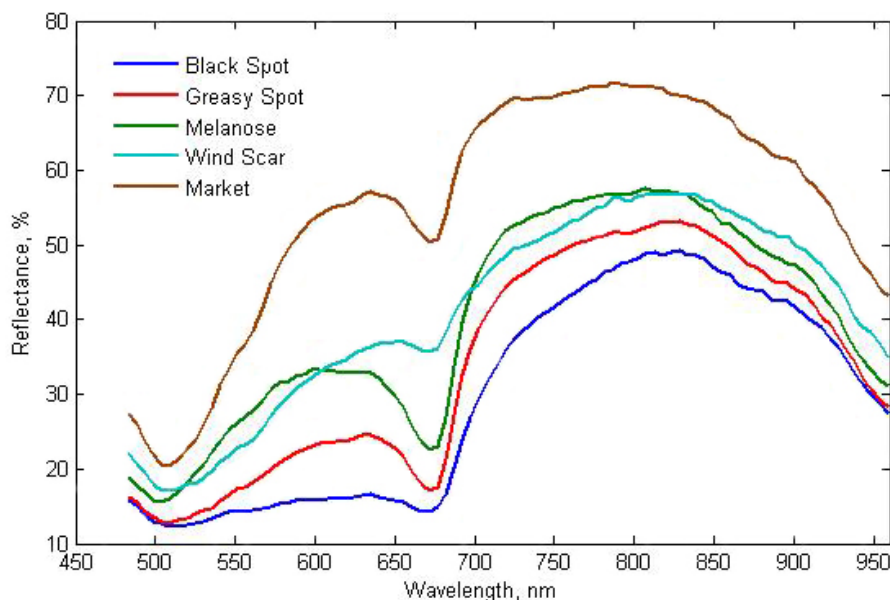

Fig. 8. The reflectance spectra of the samples with black spot, normal and different diseases over the wavelength range between 483 and 959 nm.

Table 2. The misclassification summary using six threshold values for differentiating black spot from other conditions using Spectral Information Divergence (SID) mapping of hyperspectral images.

|	SID						
Misclassification summary by class for various threshold values							
Threshold value	0.01	0.02	0.03	0.04	0.05	0.06	0.07
Black spot	135	66	12	3	2	2	0
Greasy spot	0	1	3	8	22	38	53
Market	0	0	0	0	1	1	1
Melanose	0	0	0	0	0	0	1
Wind scar	0	0	1	4	11	19	33
Accuracy (%)	74.28	87.24	96.95	97.14	93.14	88.57	83.24
Avg overall accuracy (%)				88.65			

studies. These will include looking into the effect of varying the illuminating source and changing the optical device to improve both reflectance and resolution of the images.

Summary and Conclusions

In this study, a hyperspectral imaging system was developed to distinguish citrus fruits exhibiting symptoms of citrus black spot (CBS) from fruits with other peel conditions. Five fruit classes were evaluated; 1) CBS, 2) greasy spot, 3) melanose, 4) wind scar, and 5) market. The fruit samples were collected from a grove near Ft. Pierce, FL and hyperspectral images were collected at the University of Florida laboratory over a spectral range of 400 nm to 900 nm. Reference spectrum of CBS was obtained from the ROIs that were manually selected from the CBS hyperspectral images.

Based on the results, a CBS classification accuracy of 97.9% was obtained using the SAM approach with an optimal threshold value of 0.09. The SID mapping had a CBS classification accuracy of 97.14% with a 0.04 optimal threshold. All melanose and market fruit samples were correctly classified using the two mapping approaches, while the accuracy for greasy spot was about 91% and wind scar was over 96%. Overall, the performances of both classification approaches in detecting CBS along with other

(a) SID classification accuracy (%) from threshold values (0.01 to 0.07)

Overall Accuracy: 88.65 %
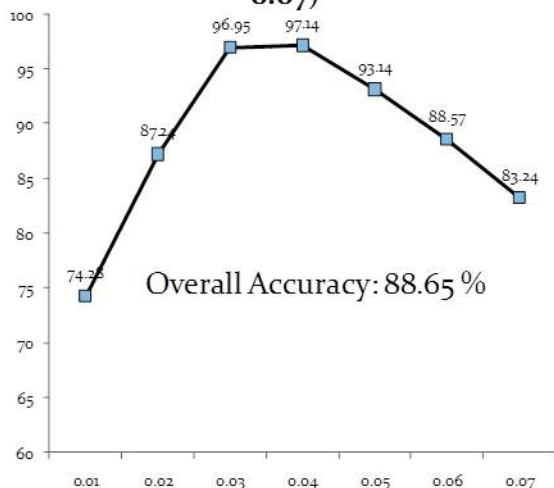
(b) SAM classification accuracy (%) from threshold values (0.06 to 0.12)
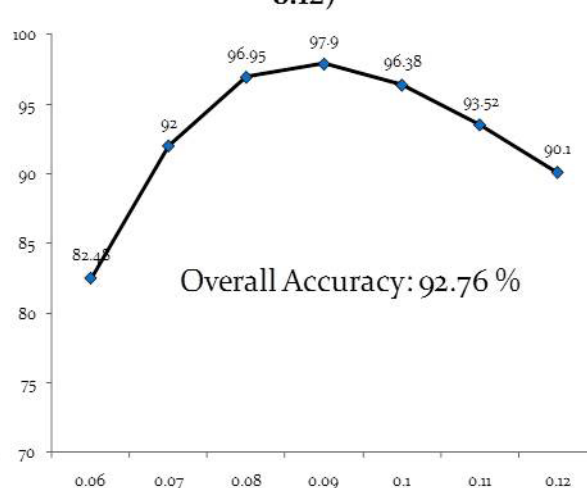
Overall Accuracy: 92.76 %

Fig. 9. Comparison with SID and SAM classification accuracy.

Table 3. The best overall classification accuracy using the Spectral Information Divergence (SID) threshold value of 0.04.

Class	Symptoms	Misclassified	Accuracy (%)	
Black spot disease	Black spot	3	98.00	98.00
No black spot disease	Greasy spot	8	91.11	
	Melanose	0	100.0	
	Wind scar	4	96.19	96.92
	Market	0	100.0	
Total		15	97.14	

Table 4. The misclassification summary using six threshold values for differentiating black spot from other conditions using Spectral Angle Mapper (SAM) mapping of hyperspectral images.

	SAM						
Misclassification summary by class for various threshold values							
Thread value	0.06	0.07	0.08	0.09	0.10	0.11	0.12
Black spot	92	42	14	3	1	1	1
Greasy spot	0	0	2	8	16	29	44
Market	0	0	0	0	0	0	1
Melanose	0	0	0	0	0	0	0
Wind scar	0	0	0	0	2	4	6
Accuracy (%)	82.48	92.00	96.95	97.90	96.38	93.52	90.10
Avg overall accuracy (%)				92.76			

Table 5. The best overall classification accuracy using the Spectral Angle Mapper (SAM) threshold value of 0.09.

Class	Symptoms	Misclassified	Accuracy (%)	
Black spot disease	Black spot	3	98.00	98.00
No black spot disease	Greasy spot	8	91.11	
	Melanose	0	100.0	97.95
	Wind scar	0	100.0	
	Market	0	100.0	
Total		11	97.90	

peel conditions were very good. However, it was found that SAM was superior to SID in threshold sensitivity. SID's performance deteriorated faster as the threshold value moves away from the optimal threshold value, while SAM's classification performance was not greatly affected as the threshold was changed.

This research demonstrated that hyperspectral imaging combined with an appropriate image processing algorithm such as SAM and SID mapping could be used for detecting CBS. Although this approach may not be appropriate for packinghouse applications, it demonstrates the potential for hyperspectral imaging to be used for identifying CBS among other confounding peel conditions. Future studies will explore the identification of significant wavelengths from the reference spectrum to develop a multispectral imaging approach that could be applied in real time on packingline applications.

Literature Cited

Burks, T.F., S.A. Shearer, and F.A. Payne. 2000. Classification of weed species using color texture features and discriminant analysis. Trans. ASAE 43(2):441–448.

Chang, C.I. 1999. Information divergence for hyperspectral image analysis. Geoscience and Remote Sensing Symp., Vol. 1:509–511.

Chung, K.T., N.A. Peres, and L.W. Timmer. 2009. Citrus disease exotic to Florida: Black spot, one of a series of the Plant Pathology Department, Florida Coop. Ext. Serv., Inst. of Food and Agr. Sci., University of Florida, p. 213.

Dewdney, M.M., 2010. Citrus black spot. Citrus Res. and Education Center, University of Florida, Citrus Ind. 91(2):19–20.

Dewdney, M.M., J.D. Yates, and M.A. Ritenour. 2011. Identification of early citrus black spot symptoms (Identificacíon de los Síntomas Iniciales de la Mancha Negra de los Cítricos). IFAS Fact Sheet PP-295. <http://edis.ifas.ufl.edu/pp285>.

Du, C.-J. and D.-W. Sun. 2006. Correlating image texture features extracted by five different methods with the tenderness of cooked pork ham: a feasibility study. Trans. ASAE 49(2):441–448.

Du, Y., C.I. Chang, H. Ren, C.-C. Chang, and J.O. Jensen. 2004. New hyperspectral discrimination measure for spectral characterization. Optical Eng. 43(8):1777–1788.

Jiang, L., B. Zhu, X. Rao, G. Berney, and Y. Tao. 2007. Black walnut shell and meat discrimination using hyper-spectral fluorescence imaging. ASABE Annu. Intl. Mtg. Paper No. 073089.

Jimenez, A.R., R Ceres, and J.L. Pons. 2000. A survey of computer vision methods for locating fruit on trees. Trans. ASAE 43(6):1911–1920.

Kim, M.S., Y.R. Chen, and P.M. Mehl. 2001. Hyperspectral reflectance and fluorence imaging system for food quality and safety. Trans. ASAE 44(3):721–729.

Lee, K.J., S. Kang, M.S. Kim, and S.H. Noh. 2005. Hyper-spectral imaging for detection defect on apple. ASABE Annu. Intl. Mtg, Paper No. 053075.

Park, B., W.R. Windham, K.C. Lawrence, and D.P. Smith. 2007. Contaminant classification of poultry hyperspectral imagery using a spectral angle mapper algorithm. Biosystems Eng. 96(3):323–333.

Pydipati, R., T.F. Burks, and W.S. Lee. 2006. Identification of citrus disease using color texture features and discriminant analysis. Computers and Electronics in Agr. 52:49–59.

Qin, J., T.F. Burks, M.A. Ritenour, and W.G. Bonn. 2009, Detection of citrus canker using hyperspectral reflectance imaging with spectral information divergence, J. Food Eng. 93:183–191.

Requnathan, M. and W.S. Lee. 2005. Citrus fruit identification and size determination using machine vision and ultrasonic sensors. ASABE Annu. Intl. Mtg. Paper No. 053017.

Shippert, P. 2003. Introduction to hyperspectral image analysis. Online J. Space Commun., Issue No. 3. http://spacejournal.ohio.edu/pdf/shippert.pdf>.

Sun, Da-Wen (ed.). (2010). Hyperspectral imaging for food quality analysis and control. Academic Press, Elsevier, San Diego. <http://www.amazon.com/Hyperspectral-Imaging-Quality-Analysis-Control/dp/0123747538>.

Tang, L., L.F. Tian, B.L. Steward, and J.F. Reid. 1999. Texture based weed classification using gabor wavelets and neural networks for real time selective herbicide application. ASABE/CSAE–SCGR Annu. Intl. Mtg. Paper No. 993036.

Zhang, Y., X.J. He, and J.H. Han. 2005. Texture feature-based image classification using wavelet package transform. ICIC 2005 part I, LNCS 3644, p. 165–173.

Yang, C., J.H. Everitt, and J.M. Bradford. 2006. Use of spectral angle mapper (SAM) and hyperspectral imagery for yield estimation. ASABE Annu. Intl. Mtg. Paper No. 061168.